IEEE Access
Multidisciplinary | Rapid Review | Open Access Journal

Received March 15, 2020, accepted March 23, 2020, date of publication March 26, 2020, date of current version April 15, 2020.

Digital Object Identifier 10.1109/ACCESS.2020.2983457

Low-Light Image Enhancement Based on Nonsubsampled Shearlet Transform

MANLI WANG[1,2], ZIJIAN TIAN[1], WEIFENG GUI[2], XIANGYANG ZHANG[2], AND WENQING WANG[3]

[1]School of Mechanical Electronic and Information Engineering, China University of Mining and Technology, Beijing 100083, China
[2]School of Physics and Electronic Information, Henan Polytechnic University, Jiaozuo 454003, China
[3]Beijing Polytechnic College, Beijing 100042, China

Corresponding authors: Zijian Tian (tianzj0726@163.com) and Weifeng Gui (guiwf0726@163.com)

This work was supported in part by the National Natural Science Foundation of China under Grant 51674269, and in part by the Key Subjects of Beijing Polytechnic College under Grant bgzyky201855z.

ABSTRACT To improve the observability of low-light images, a low-light image enhancement algorithm based on nonsubsampled shearlet transform (NSST) is presented (LIEST). The proposed algorithm can synchronously achieve contrast improvement, noise suppression, and the enhancement of specific directional details. An enhancement framework of low-light noisy images is first derived, and then, according to the framework, a low-light noisy image is decomposed into low-pass subband coefficients and bandpass direction subband coefficients by NSST. Then, in the NSST domain, an illumination map is estimated based on a bright channel of the low-pass subband coefficients, and noise is simultaneously suppressed by shrinking the bandpass direction subband coefficients. Finally, based on the estimated illumination map, the low-pass subband coefficients, and the shrunken bandpass direction subband coefficients, inverse NSST is implemented to achieve low-light image enhancement. Experiments demonstrate that the LIEST exhibits superior performance in improving contrast, suppressing noise, and highlighting specific details as compared to seven similar algorithms.

INDEX TERMS Low-light image, image enhancement, noise suppression, nonsubsampled shearlet transform, image decomposition.

I. INTRODUCTION

Low-light conditions often occur during photo shooting, such as while photographing at night time or taking pictures under trees or tunnels, etc. This leads to low image contrast and even the presence of ''black'' regions in images. Moreover, there is often noise in low-light images. To improve the visibility of low-light images, contrast improvement and noise suppression must be achieved synchronously. Low-light image enhancement [1] plays an important role in image preprocessing, as its performance directly affects the success of image processing in the next steps, including image segmentation, object detection, and image classification [2], [3], etc.

Various methods have been developed to improve the visual quality of low-light images based on different models or theories, such as histogram transforms [4]–[8], physic models [9]–[12], multi-resolution analysis theories [13], [14], and variational theories [15]–[19]. However, these methods mostly only improve the contrast, and, although noise is included in almost all low-light images, they do not exhibit good performance in noise suppression. Therefore, it is necessary to study low-light image enhancement.

Zhuang and Hao [20] used a guide filter to refine the illumination map and enhanced low-light images according to the Retinex model. Priyanka *et al.* [21] decomposed RGB images into luminance-chrominance components based on the principal component analysis framework, enhanced the contrast and brightness using the luminance component, and suppressed noise by collaboratively filtering the luminance and chrominance. Rahman *et al.* [22] jointly used Retinex and the dehazing algorithm to improve the contrast of low-light images according to the camera response model. Yu and Zhu [23] presented a physical lighting model describing poorly illuminated images, and refined the environmental light and the scattering attenuation rate by adopting a weighted guide filter to restrain the halo and block effects. Ko *et al.* [24] proposed a variational framework for low-light image enhancement via an L2 norm optimization

The associate editor coordinating the review of this manuscript and approving it for publication was Qiangqiang Yuan.

transmission map; the framework performs brightness enhancement and noise suppression.

Hao *et al.* [25], [26] presented two algorithms to enhance low-light images based on the simple Retinex model; the method presented in their earlier study improves the contrast of images in different illumination conditions, and the bright channel of the image refined by a Gaussian filter was used as the illumination of the simple Retinex model to enhance low-light images in the later study. Ma *et al.* [27] transformed RGB images into the HSI color space, and enhanced the intensity in the HSI space with a deep convolutional neural network to improve the visibility of low-light images. Tang *et al.* [28] presented a low-light enhancement method for the suppression of strong light and bright halos based on the atmospheric scattering model; the bright channel of the inverse image and nonlocal mean denoising algorithm were respectively used to suppress the strong light and noise of the enhanced image. Guo *et al.* [29] optimized the illumination map by constraining the L1 norm of the gradient of the illumination map, enhanced a low-light image according to the simple Retinex model, and suppressed the noise of the enhanced image using the BM3D denoising algorithm. Cho *et al.* [31] presented a balanced image enhancement method that both highlights image details and improves image contrast; model-based and fusion-based dehazing methods are integrated to enhance images. Li *et al.* [32] presented a robust Retinex model with noise suppression, and the illumination and reflection components are constrained by the L1 norm and Frobenius norm, respectively.

These algorithms for enhancing low-light images can be divided into two categories, namely those without noise suppression capability [20], [22], [23], [25]–[27], [31] and those with a noise suppression function [21], [24], [28], [29], [32]. However, the algorithms presented in some previous research [21], [28], [29] conduct the post-suppression of noise, that is, noise is removed after it is magnified; in these methods, the details of enhanced images may be overwhelmed by the amplified noise, leading to the impossibility of restoration. In the enhancement algorithms presented in some other studies [24], [32], detail degradation or blurring sometimes occur when noise is suppressed. Moreover, these algorithms can only enhance the image as a whole, and do not have the ability to highlight parts of details; however, it is often necessary to highlight some details that require attention.

According to the preceding analysis, this work presents a low-light image enhancement algorithm based on nonsubsampled shearlet transform (LIEST). The proposed algorithm simultaneously improves the contrast and suppresses noise, and avoids the risk of noise amplification during enhancement processing. Additionally, the algorithm can flexibly highlight details of the entire image or of selected parts.

The highlights of this paper are as follows.

1. The illumination map is estimated in the nonsubsampled shearlet transform (NSST) domain, which eliminates the noise interference.

2. The noise suppression of the enhanced image is realized by shrinking the NSST bandpass direction subband coefficients of the low-light image.

3. The enhancement algorithm proposed in this paper can not only enhance the contrast of low-light images, but can also highlight details in any specific direction.

4. The enhancement framework presented in this paper is a general framework for low-light images with noise. Not only the NSST can be used by the framework, but also other geometric multi-resolution analysis methods, such as nonsubsampled contourlet transform.

The remainder of this paper is organized as follows. The LIEST framework, which includes image decomposition, illumination map estimation, noise suppression, and enhancement image reconstruction, is described in section II. The LIEST algorithm is described in section III. The enhancement results of LIEST are provided and compared with those of other algorithms in section IV. The parameters of LIEST are analyzed in section V, and relevant conclusions are presented in section VI.

II. PROPOSED ENHANCEMENT FRAMEWORK

The Retinex model represents an observed image as the product of an illumination map and reflection component:

$$I = L \cdot R, \tag{1}$$

where the symbol I denotes the observed image, L denotes an illumination map. And the symbol R denotes the reflection component, and it is also the target recovery image; additionally, "$\cdot$" refers to element-wise multiplication. The goals of enhancement algorithms based on the Retinex model are removing the interference of the illumination map and obtaining the reflection image.

In Eq. (1), the effects of noise are not taken into account; however, low-light images often suffer from noise erosion. Therefore, after adding a noise term, Eq. (1) can be rewritten as Eq. (2):

$$I = I_l + I_h = L \cdot R_l + (L \cdot R_h + n), \tag{2}$$

where I_l and I_h respectively denote the low- and high-frequency components of the observed image I, R_l and R_h are respectively the low- and high-frequency components of the reflection component R, and n is Gaussian noise with zero mean. $I_l = L \cdot R_l$ refers to the slow-change information of I, and determines the illumination map. $I_h = L \cdot R_h + n$ is the fast-change information, and contains almost all the details and noise of I. In Eq. (2), the observed image I is uniquely given, and it can be decomposed into low-frequency components I_l and high-frequency components I_h. It is supposed that L can be obtained from I_l and n can be removed from I_h; thus, the desired image R can be expressed as follows:

$$R = R_l + R_h = \frac{I_l + (I_h - n)}{\max(L, \delta)}, \tag{3}$$

where max() is the maximum operator and δ is a small positive constant that is used to avoid a zero denominator.

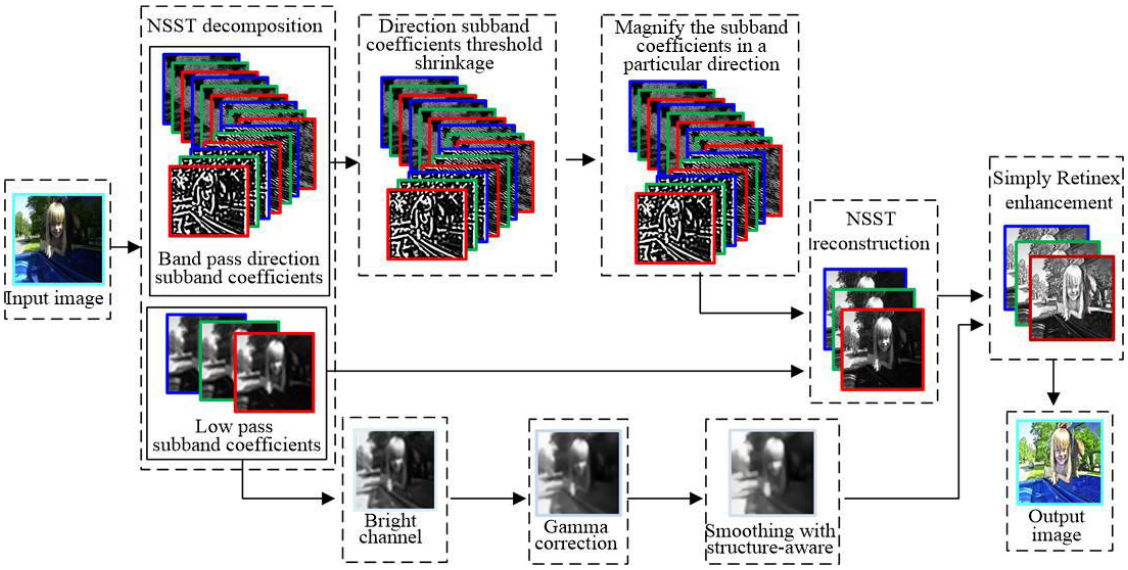

FIGURE 1. The framework of the LIEST algorithm. The red, green, and blue boxes indicate the R, G, and B color channels of the image, respectively.

According to Eq. (3), the LIEST framework for the enhancement of low-light images is designed, as presented in Fig.1.

In Fig.1, the observed image is first decomposed into low-pass subband coefficients C_l^c ($c \in \{r, g, b\}$) and bandpass direction subband coefficients C_h^c via nonsubsampled shearlet transform (NSST). The illumination map estimation is then obtained from the bright channel of C_l^c via gamma correction and structure-aware smoothing. Then, to suppress noise in the bandpass direction subband coefficients, the values below a certain threshold are set to zero by using a shrinkage approach. Finally, to highlight specific details, the bandpass direction subband coefficients are multiplied by different gains. The enhanced low-light image is reconstructed using the estimated illumination map, the low-pass subband coefficients, and the bandpass direction subband coefficients according to inverse NSST.

A. IMAGE DECOMPOSITION

NSST is used to achieve low-light image decomposition. The implementation of NSST mainly includes multi-scale decomposition and direction localization. Multi-scale decomposition is achieved by a nonsubsampled pyramid algorithm, and direction localization is realized by an improved shear filter [33], [34]. All transformations of the NSST avoid subsampling, and discrete NSST is defined as follows:

$$\left\{ \begin{array}{ll} \psi_{j,l,k} = |\det A|^{j/2} & \psi(B^l A^j x - k) \\ : j, l \in Z, k \in Z^2 & \end{array} \right\}, \tag{4}$$

where A is an anisotropic dilation matrix and B is a shear matrix; they are respectively defined as $A = \begin{pmatrix} 4 & 0 \\ 0 & 2 \end{pmatrix}$ and $B = \begin{pmatrix} 1 & 1 \\ 0 & 1 \end{pmatrix}$.

For the appropriate choices of ψ, the discrete nonsubsampled shearlet forms a Parseval frame (tight frame) for $L^2(R^2)$. Therefore, the reconstruction formula corresponding to Eq. (4) is defined as follows:

$$f = \sum_{j,l \in Z, k \in R^2} \langle f, \psi_{j,l,k} \rangle \psi_{j,l,k}. \tag{5}$$

For convenience, the NSST operation is recorded as $T_{NSST}()$, and the inverse NSST operation is recorded as $T_{NSST}^{-1}()$. Then, a low-light image is decomposed by NSST, which can be denoted as follows:

$$T_{NSST}(I^c) = \left\{ \begin{array}{l} C_l^c, C_{h,j,s}^c, j = 1, 2, \ldots, J, \\ s = 1, 2, \ldots, S_j \end{array} \right\}, \tag{6}$$

where C_l^c and $C_{h,j,s}^c$ are respectively low-pass and bandpass direction subband coefficients of the low-light image I^c, c denotes the RBG color channel, J is the maximum of the decomposition scales, and S_j is the direction number of the j-th decomposition scale. Additionally, $\{C_l^c, C_{h,j,s}^c\}$ denotes the set of all the decomposition coefficients of I^c. When $C_l^c = I_l^c$, the illumination map can be obtained from C_l^c.

B. ILLUMINATION MAP ESTIMATION

According to analyses of Eqs. (2) and (6), the bright channel of the low-pass subband coefficients C_l^c can be regarded as an initial illumination map $\tilde{L}$:

$$\tilde{L} = \max_{c \in \{r,g,b\}} (C_l^c, \varepsilon), \tag{7}$$

where max() is the maximum operator, ε is a small positive constant that prevents the existence of a zero value in $\tilde{L}$, and the recommended value range is [0.01,0.1].

$\tilde{L}$ is directly used as an illumination map; if its grayscale is too low, the enhanced image will have an excessively high

contrast. Therefore, it is necessary to improve the grayscale of $\tilde{L}$ via gamma correction, as given by Eq. (8):

$$L_G = \left(\tilde{L}\right)^{\gamma}. \tag{8}$$

The value of the L_G is appropriate for use as the illumination map; however, there is still a small amount of details in the L_G, which does not satisfy the smoothing characteristic of the illumination map. To smooth the L_G and preserve its structure, the structure-aware smoothing solver presented in a previous work [27] is used. The solver is defined as follows:

$$\min_{\hat{L}} \left\| L_G(x) - \hat{L}(x) \right\|_F^2 + \alpha \sum_x \sum_{d\in\{h,v\}} \frac{W_d(x)(\nabla_d \hat{L}(x))^2}{|\nabla_d L_G(x)| + \varepsilon}, \tag{9}$$

where α is the balance coefficient, ε is a small constant to prevent a zero denominator, $\hat{L}$ is the target illumination, $\|\cdot\|_F$ denotes the Frobenius norm, and ∇_d contains ∇_h (horizontal) and ∇_v (vertical), and is a first-order difference operator. Additionally, $W_d(x)$ includes $W_h(x)$ (horizontal) and $W_v(x)$ (vertical), and is a weight matrix that is defined by the following:

$$W_d(x) = \sum_{y\in\Omega(x)} \frac{G_\sigma(x,y)}{|\sum_{y\in\Omega(x)} G_\sigma(x,y)\nabla_d L_G(y)| + \varepsilon}, d \in \{h, v\} \tag{10}$$

where $\Omega(x)$ is a local window centered at pixel x, y is an index in the $\Omega(x)$. $G_\sigma(x, y)$ is generated by a Gaussian kernel function with the standard deviation of σ. Throughout this work, $\sigma = 2$ is set. $|\cdot|$ is the absolute value operator. $G_\sigma(x, y)$ is given by Eq. (11):

$$G_\sigma(x,y) \propto \exp\left(-dist(x,y) \Big/ -2\sigma^2\right), \tag{11}$$

where $dist(x, y)$ is the spatial Euclidean distance between pixels x and y.

According to Eqs. (10) and (11), Eq. (9) only contains quadratic terms. Thus, referring to previous work [29], [30], the value of $\hat{L}$ that minimizes Eq. (9) is uniquely defined as the solution of Eq. (12):

$$(\mathbf{I} + \sum_{d\in\{h,v\}} \boldsymbol{D}_d^T Diag(\tilde{\boldsymbol{W}}_d)\boldsymbol{D}_d)\hat{L} = L_G, \tag{12}$$

where the symbol $\boldsymbol{D}_d$ denotes forward difference operator, and $\tilde{\boldsymbol{W}}_d$ is vectorized with $\tilde{\boldsymbol{W}}_d \leftarrow \frac{W_d(x)}{|\nabla_d L_G(x)|+\varepsilon}$, and the operator $Diag(\tilde{W}_d)$ constructs a diagonal matrix using $\tilde{W}_d$. Because $(\boldsymbol{I} + \sum_{d\in\{h,v\}} \boldsymbol{D}_d^T Diag(\tilde{\boldsymbol{W}}_d)\boldsymbol{D}_d)$ is a symmetric positive definite Laplacian matrix, there are many techniques available for solving it, such as that presented by Farbman *et al.* [30].

According to the aforementioned conditions, $\hat{L}$ can be easily obtained by solving quadratic terms, and is used as the final illumination map of the proposed enhancement framework.

Different enhancement results of images of potted plants were obtained by using $\tilde{L}$, L_G, and $\hat{L}$, respectively, as presented in Fig. 2.

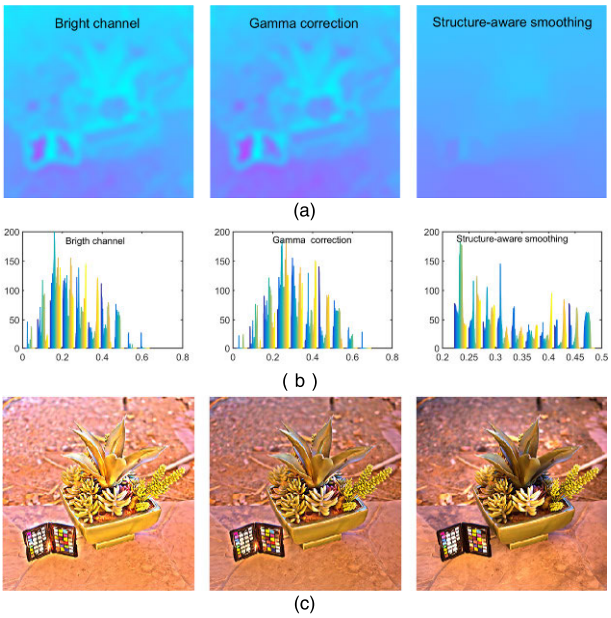

FIGURE 2. Enhanced images with different illumination maps. (a) Different illumination maps; (b) Histograms of (a); (c) Enhanced images corresponding to (a).

From left to right, Fig. 2(a) presents the images obtained using $\tilde{L}$, L_G, and $\hat{L}$. Fig. 2(b) presents the histograms of the illumination maps in Fig. 2(a), and Fig. 2(c) presents the enhanced images corresponding to Fig. 2(a).

It is evident that, after gamma correction and structure-aware smoothing, the histograms gradually became larger and more uniform, and the contrast and details of the enhanced images became better.

C. NOISE SUPPRESSION

After obtaining the illumination maps, noise suppression in bandpass direction subband coefficients is the key task to obtaining good-quality enhanced images.

According to the multiresolution analysis theory, NSST concentrates image features in a few large-magnitude NSST coefficients, and in $C^c_{h,j,s}$, the values of noise are much smaller than the values of image detail features. Therefore, the numerical values in $C^c_{h,j,s}$ corresponding to noise are set to zero by using the threshold function Eq. (13), which can achieve noise suppression without affecting the image quality.

$$\hat{C}^c_{h,j,s} = \begin{cases} C^c_{h,j,s}, & \left|C^c_{h,j,s}\right| > k_j \sigma^c \hat{\sigma}^c_{j,s}, \quad c \in \{r, g, b\} \\ 0, & \text{others}, \end{cases} \tag{13}$$

where k_j is a threshold coefficient of the j-th decomposition scale, and its value is set with the mean of the Gaussian distribution as the center and 3 times variance as the amplitude. Additionally, σ^c denotes the noise variance of a color channel of the original image, and is calculated by the wavelet noise estimation equation (14). $\hat{\sigma}_{j,s}$ is the variance of the bandpass direction subband coefficient matrix of the j-th decomposition scale and the s-th direction, and $\hat{\sigma}_{j,s}$ can be obtained by

FIGURE 3. Comparison of enhancement effects with and without noise suppression. (a) A low-light image with a Gaussian noise variance of 10; (b) Enhanced image without noise suppression; (c) Enhanced image of (a) with noise suppression.

the Monte Carlo method.

$$\sigma^c = \max\left(\beta, \frac{med(|W_{d1}^c|)}{0.6745}\right), c \in \{r, g, b\}, \quad (14)$$

where $med()$ denotes the median operation, $||$ denotes the absolute value operation, W_{d1} is a diagonal wavelet coefficient matrix of the single-scale wavelet decomposition I^c; in this paper, the "sym4" wavelet is used to decompose I^c. Additionally, β is a small positive constant that prevents the threshold from being too low, and its recommended value range is [0.001,0.01].

The calculation steps of $\hat{\sigma}_{j,s}^c$ are as follows.

First, the unit standard deviation matrix N_1 is generated by using a pseudorandom algorithm, and has the same size as I^c. Then, N_1 is decomposed by "à trous" wavelet transform, and its scales and directions are the same as those of the NSST decomposition I^c. Finally, noise variances of the "à trous" wavelet coefficients are calculated by the wavelet noise estimation formula, and these variances are the corresponding $\hat{\sigma}_{j,s}^c$.

If specific details do not need to be highlighted separately, and according to $\hat{L}$ and the inverse NSST of $\{C_l^c, \hat{C}_{h,j,s}^c\}$, the enhancement image can be obtained by Eq. (3).

Different enhancement effects using the same illumination map are presented in Fig. 3. The NSST decomposition coefficients of the image in Fig. 3(c) have been shrunk, while those in Fig. 3(b) have not.

As presented in Fig. 3(b), the noise of the enhanced image was greatly amplified with the contrast improvement, and its variance reached 19.5. However, the noise of the enhanced image in Fig. 3(c) was effectively suppressed, and its variance was only 1.3.

It is evident that the synchronous noise suppression method can effectively suppress the noise of the enhanced image, and avoids the risk of amplifying noise during the contrast improvement process.

D. ENHANCED IMAGE RECONSTRUCTION

It is sometimes necessary not only to enhance the overall contrast and details of an image, but also to highlight the specific direction details of an image. Therefore, before the implementation of the inverse NSST, the specific bandpass direction subband coefficients in $\hat{C}_{h,j,s}^c$ must be amplified to achieve the highlighting of specific details.

Based on the preceding analyses, the reconstruction formula of an enhanced image is designed as follows:

$$I_e^c = \frac{T_{NSST}^{-1}\left(\left\{C_l^c, K_{j,s}^c \cdot \hat{C}_{h,j,s}^c, \atop j = 1, 2, \ldots, J, s = 1, 2, \ldots, S_j\right\}\right)}{\max(\hat{L}, \delta)}, \quad (15)$$

where I_e^c denotes a color channel of the enhanced image, $K_{j,s}^c$ is the gain of bandpass direction subband coefficients, the recommended value range of which is [1], [5], and T_{NSST}^{-1} denotes the inverse NSST operation. The other symbols have the same definitions as those in Eqs. (3) and (6). Additionally, $\left\{C_l^c, K_{j,s}^c \hat{C}_{h,j,s}^c, j = 1, 2, \ldots, J, s = 1, 2, \ldots, S_j\right\}$ is a set of all subband coefficients, and $\delta = 0.01$ is recommended.

III. LIEST ALGORITHM

The proposed LIEST algorithm mainly includes three steps: decomposing the low-light image and shrinking the bandpass direction subband coefficients, estimating the illumination map, and reconstructing the enhanced image.

Algorithm 1 Low-Light Image Enhancement based on Nonsubsampled Shearlet Transform

Input: Low-light color image I
Initialization: Assigning values to all the parameters
Step 1 While $c \in \{r, g, b\}$, do
1. Decomposing I^c using NSST
2. Computing σ^c and $\hat{\sigma}_{j,s}$
3. Shrinking $C_{h,j,s}^c$ and obtaining $\hat{C}_{h,j,s}^c$
4. Calculating $K_{j,s} \cdot C_{h,j,s}^c$

End
Step 2 Calculating $\hat{L}$ using C_l^c
Step 3 While $c \in \{r, g, b\}$, do
1. Performing inverse NSST using $C_l^c, K_{j,s} \cdot C_{h,j,s}^c$
2. Calculating enhanced color image I_e^c.

End
Output: Enhanced color image I_e

IV. EXPERIMENTS

In this section, some image quality evaluation indexes are provided, as are their definitions. Next, an analysis of the proposed enhancement framework, including the illumination map estimation, the highlighting of specific details, and noise suppression, is given. The proposed LIEST algorithm is then qualitatively and quantitatively compared with other state-of-the-art algorithms, including Simultaneous Reflection and Illumination Estimation (SRIE) [19], Low-light Image Enhancement via Illumination Map Estimation (LIME) [29], Structure-Revealing Low-light Image Enhancement (SRLIE) [32], McCann Retinex (MCR) [35], the Naturalness Preserved Enhancement (NPE) algorithm [36], Low-light Image Enhancement using the Camera Response Model (LECARM) [37], and a Hybrid L2-Lp Variational Model (HVM) for single low-light image enhancement with bright channel prior [38].

All the code was run in MATLAB R2014b, and all the experiments were conducted on a PC running Windows 10 with 16G RAM and 2.7GHz i7 CPU.

In the experiment, the low-light images were selected from image sets of previous research [19], [39], [40], and a total of 2162 images with an average size of 676 × 675 were used.

A. IMAGE QUALITY EVALUATION INDEXES

To quantitatively evaluate the enhancement performances of the LIEST algorithm, the noise variance (recorded as Sigma^2), mean local standard deviation (MLSD), mean local entropy (MLE), and Brenner gradient (BG) were used to evaluate the noise levels, contrast, details, and clarity of the enhanced images.

In addition to these evaluation indexes, to further comprehensively evaluate the quality of the enhanced images, the blind image quality evaluation indexes NIQE [41] and BRIS [42] were also used.

The mean local standard deviation is the average of the local standard deviation; the larger its value, the higher the contrast of the image. The local standard deviation is defined as follows:

$$LSD(w) = \sqrt{\frac{1}{n-1}\left[\sum_{x,y\in w} f(x,y)^2 - \frac{1}{n}\left(\sum_{x,y\in w} f(x,y)\right)^2\right]}, \quad (16)$$

where w is a small neighborhood with the size $(2d+1)\times(2d+1)$, n is the total number of pixels contained in w, and, in this work, $d = 1, n = 3 \times 3$. Additionally, f is the evaluated image.

The mean local entropy is the average of the local entropy; the larger its value, the richer the textures or details. If a small neighborhood w with the size of $m \times n$ is defined, then the local entropy is defined as follows:

$$\begin{cases} LE(w) = -\sum_{r=0}^{r_{\max}} p(r)\log(p(r)) \\ p(r) = n(r)/m \times n, \end{cases} \quad (17)$$

where $p(r)$ is the probability that grayscale r appears in w, $n(r)$ is the number of pixels with grayscale r, and $r_{\max}$ is the maximal grayscale.

The Brenner gradient is used to judge the clarity of the image; the larger its value, the clearer the image. If an image has a size of $m \times n$, then the Brenner gradient is defined as follows:

$$\begin{cases} BG(f) = \frac{1}{mn}\sum_{x=1}^{m-2}\sum_{y=1}^{n} t(x,y), t > thr \\ t(x,y) = (f(x+2,y) - f(x,y))^2, \end{cases} \quad (18)$$

where BG denotes the Brenner gradient and thr denotes a set limit; in this, paper $thr = 4$.

In this work, noise variance is estimated by the wavelet noise estimation formula.

These indexes were used to evaluate the enhanced images, as presented in the subsequent section.

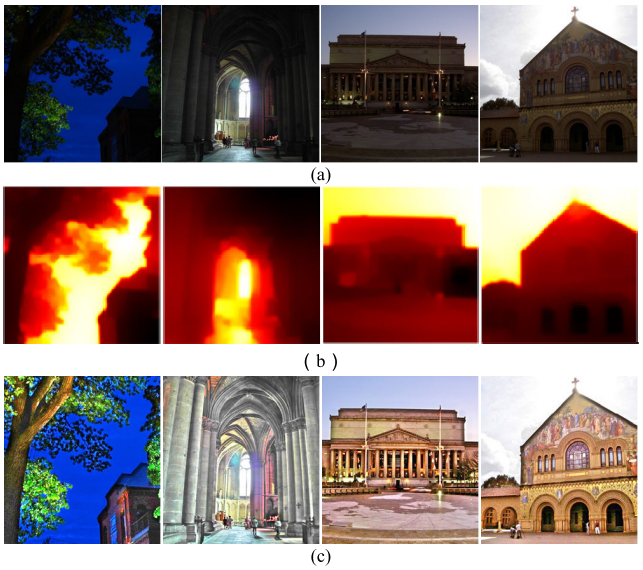

FIGURE 4. Comparison results between the original and enhanced images. (a) Low-light images; (b) Illumination maps; (c) Enhanced images.

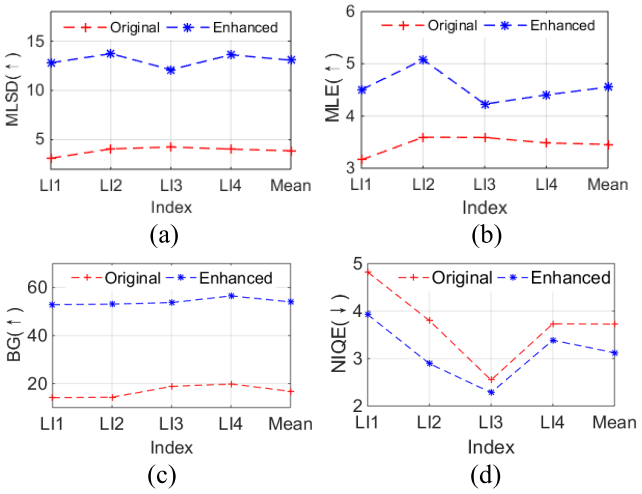

FIGURE 5. Comparison between the evaluation indexes of the original and enhanced images; the comparisons of (a) MLSD, (b) MLE, (c) BG, and (d) NIQE.

B. ILLUMINATION ESTIMATION AND THE HIGHLIGHTING OF SPECIFIC DETAILS

The illumination map estimation method and the detail-highlighting performance of the LIEST algorithm were tested, and the enhanced image qualities were evaluated both visually and quantitatively.

In the experiment, the NSST was used to decompose the low-light images LI1-LI4 with four scales, and the number of directions corresponding to each scale was 8, 8, 16, and 16, respectively. The other parameters of the LIEST were set as follows: $\beta = 0.0035$, $k_j = [0, 2.4, 2.4, 3]$, $\delta = 0.005$, $\alpha = 0.015$, and $\gamma = 0.8$.

The enhanced images of LI1-LI4 and their corresponding illumination maps are shown in Fig. 4.

In each line of Fig. 4, the images from left to right respectively correspond to LI1 to LI4.

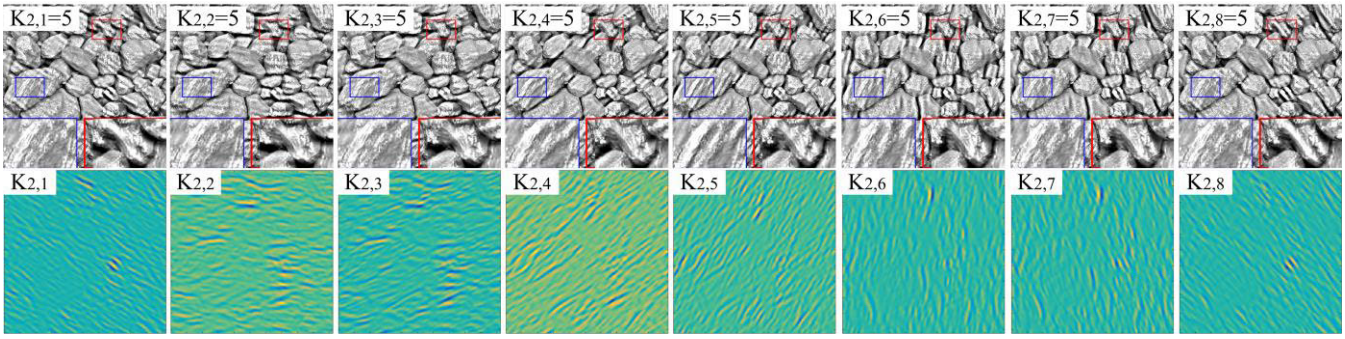

FIGURE 6. Enhancement effects with different band direction gains. (a) The enhanced images with different band direction gains; (b) Different frequency band directions of images in (a).

As presented in Fig. 4(b), the estimated illumination maps of different low-light images were very smooth, and the main structures of the original images were retained. These features meet the requirements of the Retinex theoretical illumination map. The ''black'' regions of the original images are clear in the enhanced images in Figs. 4(c) and 4(a), which demonstrates that the enhancements of these low-light images were realized by using the illumination maps estimated in the NSST domain.

In addition to visual evaluation, to further objectively evaluate the proposed illumination map estimation method, the MLSD, MLE, BG, and NIQE values of the enhanced images are presented in Fig. 5.

As presented in Figs. 5(a-c), compared with the values of the original images, the values of the enhanced images were improved significantly, thereby verifying the great improvements in the contrast, entropy, and clarity of the enhanced images; for the same noise level, the higher the contrast and clarity, the better the observability of the image, and the higher the entropy, the richer the details of the image. As revealed in Fig. 5(d), the values of the original images were reduced as compared to those of the enhanced images; however, the smaller the NIQE value, the better the comprehensive quality of an image.

Therefore, Fig. 5 proves that the qualities of the images enhanced by the LIEST algorithm were improved greatly, and that the illumination map estimation method in the NSST domain is very effective.

To verify the detail-highlighting performance of the LIEST, an image of stones was enhanced by the LIEST with different gains of bandpass direction subband coefficients, and the other parameters, excluding $K_{j,s}^{c}$, were kept the same. The experimental results are presented in Fig. 6, which only shows the results of eight different bandpass direction subband coefficient gains; the other gains were all equal to 1, excluding the gain marked in the picture. The first line in Fig. 6 presents the different enhanced images, and the other line presents the corresponding subband directions.

It is evident from Fig. 6 that different direction details of the enhanced images were highlighted when different bandpass direction gains were used. Additionally, the numbers of the direction filters of NSST were unlimited, and therefore the selected frequency direction was unlimited. Thus, the LIEST can highlight the details in any frequency directional subband, which can be picked out by direction filters of NSST.

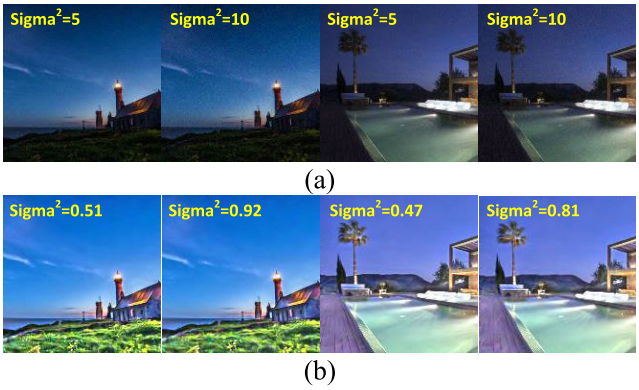

FIGURE 7. Enhancement effects of images with different noise variances. (a) Original images with different noise variances; (b) Enhanced images with noise suppression.

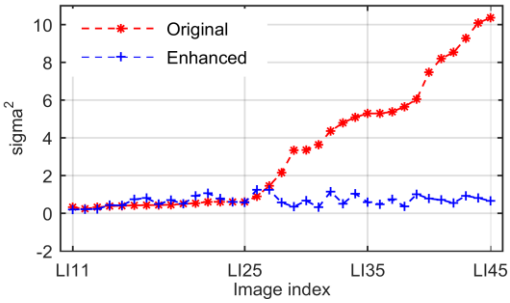

FIGURE 8. Noise variance statistics of the original and enhanced images.

C. NOISE SUPPRESSION

This section verifies the noise suppression performance of the LIEST algorithm.

The low-light images LI5 and LI6 with Gaussian noise variances 5 and 10 were first enhanced by the LIEST algorithm, and the results are presented in Fig. 7.

Fig. 7(a) presents the original images, and Fig. 7(b) presents the enhanced images. Additionally, the noise variance of each image is denoted. As compared with the images in Fig. 7(a), the contrasts and details of the enhanced images

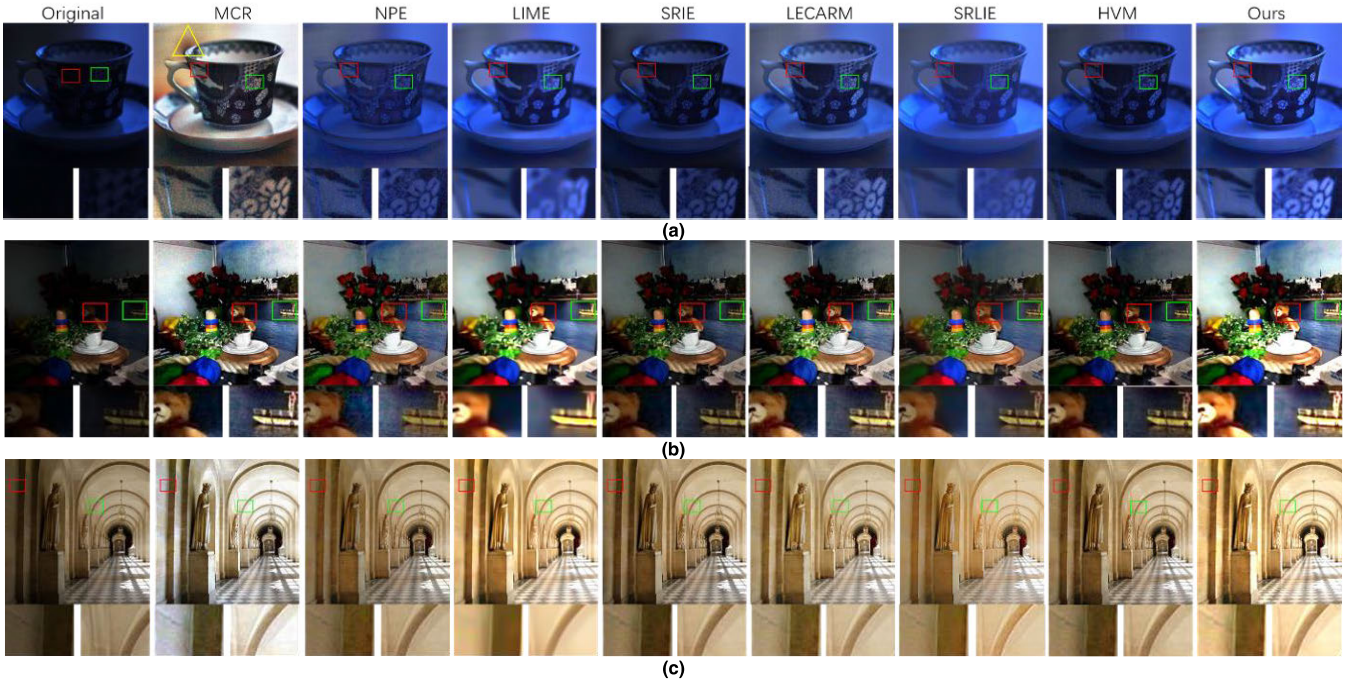

FIGURE 9. Comparison of the proposed enhancement algorithm with seven state-of-the-art algorithms. (a) Comparisons of the enhanced results of image LI60; (b) Comparisons of the enhanced results of image LI61; (c) Comparisons of the enhanced results of image LI62.

in Fig. 7(b) were all improved. It is evident that the same enhanced images with different noise variances were visually unchanged and their noise residuals were slightly different, but their variance levels were all below 1.

To test the noise suppression stability of the LIEST algorithm, it was used to enhance 36 low-light images with different noise variances. The noise variances of the original images and the enhanced images are recorded statistically in Fig. 8.

In Fig. 8, the red stars denote the variances of the original images, and the blue crosses denote the variances of the enhanced images. The line formed by the blue crosses is basically horizontal, and it does not fluctuate with the red line; this demonstrates the stable performance of the noise suppression effect of the LIEST.

D. COMPARISON OF DIFFERENT ALGORITHMS

The performance of the proposed image enhancement algorithm was compared with the performances of other state-of-art algorithms, namely MCR, NPE, LIME, SRIE, LECARM, SRLIE, and HVM.

To compare the eight enhancement algorithms, two experiments were conducted. The first was the comparison of the enhancement of low-light, clean images (Gaussian noise variance of less than 1), and the second was the comparison of the enhancement of low-light, noisy images (Gaussian noise variance of greater than 2).

The enhancement results of the low-light, clean images LI60, LI61, and LI62, which had noise variances of 0.7, 0.5, and 0.52, respectively, are presented in Fig. 9.

In each row in Fig. 9, the top images are the original image and those enhanced by different algorithms, and the bottom images are magnified details of the top images.

In Fig. 9(a), there is obvious color distortion (the triangular region) in the MCR-enhanced image. The images enhanced by the LIME and SRLIE algorithms were excessively smoothed due to the effects of noise suppression. The contrasts of the images enhanced by the NPE, SRIE, and HVM algorithms were lower than images enhanced by the other algorithms. The overall enhancement effect of the LECARM algorithm was similar to that of the proposed algorithm; however, it is evident from the local magnified details that there was less noise in the image enhanced using the proposed method. Therefore, the comparisons of the enhancement of image LI60 reveal that the effects of the proposed algorithm were the best.

As revealed in Fig. 9(b), the enhancement effects of the eight algorithms were similar; however, it is clear from the magnified details that the image enhanced by the proposed algorithm was the clearest.

As presented in Fig. 9(c), comparing with the original image, color deviation occurred in the image enhanced by the MCR algorithm, and the contrasts of the images enhanced by the NPE and SRIE algorithms were improved less. There was obvious detail loss in the image enhanced by the LIME algorithm. The images enhanced by the other three algorithms were visually similar.

Based on all the visual comparisons, it is clear that the proposed algorithm presented advantages in enhancing low-light images.

TABLE 1. Evaluation data of the LI60 enhanced images.

Algorithm	Sigma^2 (↓)	NIQE (↓)	MLSD (↑)	MLE (↑)	BG (↑)
MCR	3.86	***3.98***	**10.35**	**4.07**	**56.28**
NPE	2.49	3.99	***6.08***	***3.99***	***27.95***
LIME	1.15	7.66	4.34	3.49	9.11
SRIE	1.40	4.56	3.84	3.57	12.93
LECARM	2.37	4.12	5.91	3.29	26.87
SRLIE	***0.46***	5.09	2.48	3.12	5.96
HVM	1.61	4.33	4.49	3.66	16.61
LIEST	**0.37**	**3.05**	5.11	3.85	19.46

TABLE 2. Evaluation data of the LI61 enhanced images.

Algorithm	Sigma^2 (↓)	NIQE (↓)	MLSD (↑)	MLE (↑)	BG (↑)
MCR	2.78	**2.32**	**12.07**	4.10	**53.77**
NPE	2.29	***2.34***	9.06	4.03	45.78
LIME	0.60	6.06	7.69	***4.11***	32.60
SRIE	1.26	2.87	6.57	3.82	32.22
LECARM	1.95	2.86	9.31	3.21	43.11
SRLIE	***0.53***	3.74	6.15	3.92	26.56
HVM	1.23	2.87	7.17	3.87	35.03
LIEST	**0.37**	2.88	***11.87***	**4.41**	***45.83***

TABLE 3. Evaluation data of the LI62 enhanced images.

Algorithm	Sigma^2 (↓)	NIQE (↓)	MLSD (↑)	MLE (↑)	BG (↑)
MCR	1.19	**2.96**	**10.23**	**4.50**	**34.37**
NPE	0.90	3.28	6.93	4.26	25.76
LIME	**0.16**	5.68	6.89	4.03	20.41
SRIE	0.69	3.47	7.37	4.36	25.17
LECARM	0.96	***3.13***	8.27	4.36	29.35
SRLIE	0.75	3.67	8.07	4.31	25.99
HVM	0.86	3.11	8.16	4.25	29.85
LIEST	***0.20***	3.33	***9.89***	***4.41***	***31.60***

In addition to the visual comparisons, quantitative comparisons of the eight algorithms were made. The Sigma^2, MLSD, MLE, BG, and NIQE indexes of the images LI60, LI61, and LI62 enhanced by the different algorithms are respectively provided in Tables 1, 2, and 3.

In all the tables, underlined and italicized numbers represent the optimal values and suboptimal values, respectively. The ↓ symbol indicates that the smaller the value, the better, and the ↑ symbol indicates the larger the value, the better.

Table 1 reveals that the MLSD, MLE, and BG values of the MCR algorithm were optimal, its NIQE value was suboptimal, and its Sigma^2 value was the worst; these findings indicate that the MCR algorithm was optimal for improving contrast, but its comprehensive effect on enhancing the low-light image was not the best. For the proposed LIEST algorithm, the Sigma^2 and NIQE values were optimal, which demonstrates the superiority of the enhanced image. Considering the effect of amplified noise, as compared with the original noise variance of 0.7, the Sigma^2 indexes of the enhancement images of the MCR, NPE, LECARM, and HVM algorithms were obviously magnified. As compared with the remaining algorithms, the evaluation indexes of the image enhanced by the LIEST algorithm were all the best. According to these comparisons, for the enhancement of image LI60, the performance of the LIEST algorithm was the best of all eight tested algorithms.

As presented in Table 2, the NIQE, MLSD, and BG values of the MCR algorithm were optimal, its MLE value was the third-best, but its Sigma^2 value was the worst; these findings demonstrate that the MCR algorithm was optimal for improving contrast, but its noise-suppression effect was the worst. The Sigma^2 and MLE values of the LIEST algorithm were optimal, but the MLSD and BG were suboptimal. Considering the effect of amplified noise, as compared with the original noise variance 0.5, the Sigma^2 indexes of the images enhanced by the MCR, NPE, and LECARM algorithms were obviously magnified. Additionally, as compared with the remaining algorithms, the NIQE value of the LIEST was suboptimal, and the values of the rest of the indicators were optimal. According to these comparisons, for the enhancement of image LI61, the performance of the LIEST algorithm was close to that of the MCR algorithm.

As presented in Table 3, there were four suboptimal indexes of the LIEST-enhanced image, and its NIQE value was the sixth. If noise variance is taken into account, as compared with the variance of the original image, the MCR, NPE, and LECARM algorithms magnified the noise variance nearly twofold. If these three algorithms are not considered, then there are four optimal indexes of the image enhanced by the LIEST algorithm, and its Sigma^2 value was slightly larger than that of the LIME algorithm. According to these comparisons, for the enhancement of image LI62, the performance of the LIEST algorithm was close to that of the MCR algorithm.

According to the visual comparisons of the LI60, LI61, and LI62 images, the LIEST has the most stable enhancement performance in visual. Based on the objective data comparisons of the LI60, LI61, and LI62 images, of the eight algorithms, the enhancement performance of the LIEST is close to the MCR. However, the MCR algorithm causes different levels of noise amplification, which has no ability to suppress noise.

Based on the comparative analysis of visual and objective data, the LIEST has the better comprehensive performance in enhancing clean, low-light images.

The performances of the eight algorithms in enhancing noisy images were compared.

The enhancement results of the low-light noisy images LI63, LI64, and LI65, which had noise variances of 3.1, 5.0, and 5.1, respectively, are presented in Fig. 10, in which the first row presents the original image and the different enhanced LI63 images, and the middle and last rows respectively correspond to images LI64 and LI65.

As revealed in Fig. 10, the contrasts of the LI63 images enhanced by the MCR, SRIE, and HVM algorithms remained low, and the detail loss of the images enhanced by the LIME algorithm was serious. The other four enhanced images were visually similar; however, the image enhanced by the proposed algorithm was the clearest.

The contrasts of the LI64 images enhanced by the MCR, SRIE, and HVM algorithms remained low. As can be determined by their local magnified images, the detail loss of the images enhanced by the LIME algorithm was serious, and the noise of the images enhanced by the NPE, LECARM,

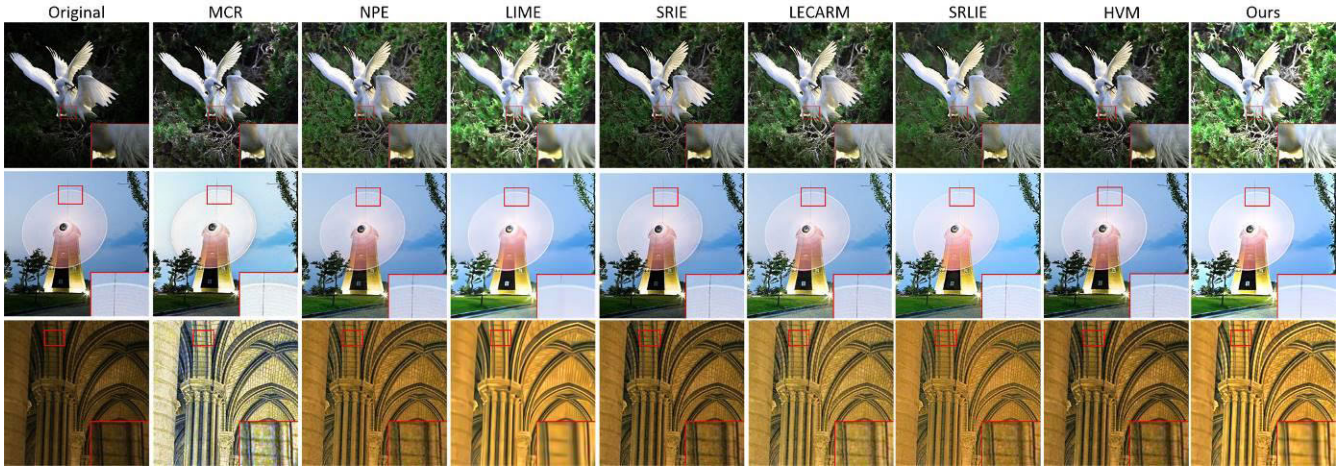

FIGURE 10. Comparisons of the eight algorithms in enhancing noisy images.

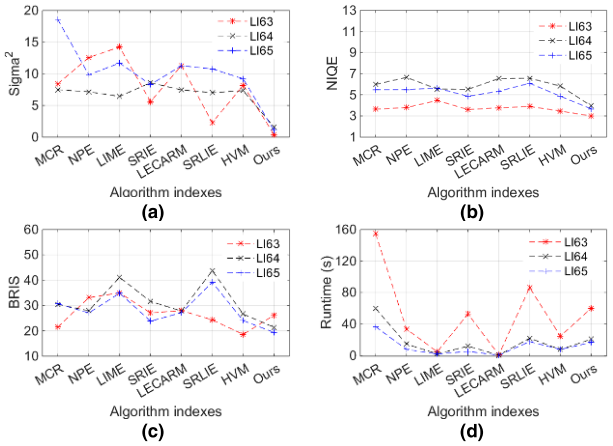

FIGURE 11. Evaluations of the noisy images enhanced using the eight algorithms. (a) Sigma^2, (b) NIQE, (c) BRIS, and (d) runtimes of the seven algorithms.

and SRLIE algorithms was obviously magnified. The image enhanced by the proposed algorithm had the least amount of noise, and its details and contrast were the best.

As can be determined by the local magnified images of the enhanced LI65 images, the noise of the images enhanced by the MCR, NPE, SRIE, LECARM, SRLIE, and HVM algorithms was obviously magnified, and detail loss of the image enhanced by the LIME algorithm was serious. Visually, the image enhanced by the proposed algorithm was the best.

According to Fig. 10, of the eight tested algorithms, the proposed algorithm had the best visual effect.

The MLSD, MLE, and BG evaluation indexes may be influenced by large amounts of noise. Therefore, to further quantitatively compare the different enhanced LI63, LI64, and LI65 images, the Sigma^2, NIQE, and BRIS indexes were used to evaluate the enhanced noisy images. The runtime, Sigma^2, NIQE, and BRIS evaluations of the enhanced noisy images are presented in Fig. 11.

As presented in Fig. 11, the values of the Sigma^2, NIQE, BRIS, and runtime evaluation indexes are optimal when they are as small as possible.

In Figs. 11(a) and 11(b), the Sigma^2 and NIQE values of the images enhanced by the LIEST algorithm were the smallest, and their values were relatively concentrated; this demonstrates that, based on these two indexes, the performance of the LIEST algorithm was better than that of other seven algorithms.

Fig. 11 (c) compares the BRIS evaluation indexes of the enhanced LI64 and LI65 images, and it is evident that the evaluation index of the proposed algorithm was the best. The evaluation index of the proposed method for the enhanced LI63 image was in the middle, and the value was greater than the values for the MCR, SRLIE, and HVM algorithm. As revealed by Fig. 11(d), the order of the mean runtime of the eight algorithms from least to greatest was as follows: LECARM < LIME < HVM < NPE < SRIE < LIEST < SRLIE < MCR.

The computational complexity of the LIEST algorithm is determined by the illumination map estimation and noise suppression. The computational complexity of the illumination map estimation is $O(1)$, the computational complexity of the noise suppression based on NSST is $O(n^2 \log n)$, and the overall computational complexity of the LIEST algorithm is about $3 \times O(n^2 \log n)$.

According to the visual comparison and objective data comparison of the enhanced clean and noisy images, it is demonstrated that, among the eight tested algorithms, the LIEST presented the best comprehensive performance in enhancing the low-light images.

V. PARAMETER ANALYSES AND DISCUSSION

A. PARAMETERS RELATED TO ILLUMINATION MAP

This section discusses the parameters related to estimating the illumination map, including ε in Eq. (7), γ in Eq. (8), and α in Eq. (9).

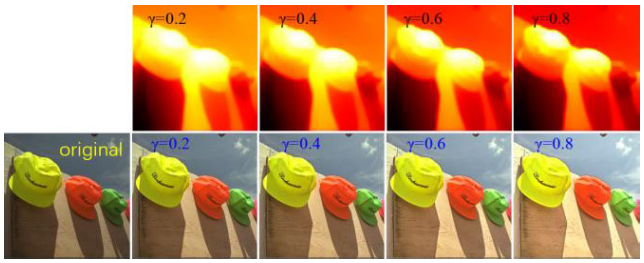

FIGURE 12. Enhanced images using different γ values.

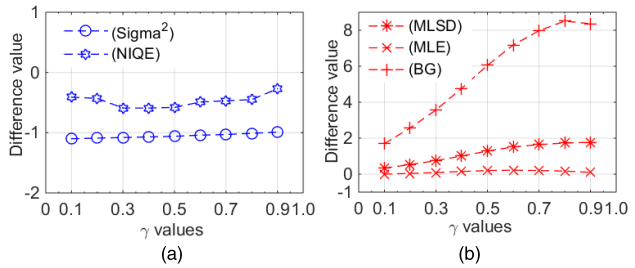

FIGURE 13. Difference value curves for the evaluation indicators of the original and enhanced images with different γ values. (a) Difference value curves for Sigma^2 and NIQE; (b) Difference value curves for MLSD, MLE, and BG.

The role of ε is to prevent the denominator from being zero, and it also determines the maximum magnification. In the range of the recommended values, it has little effect on the enhanced image; it will therefore not be discussed further here.

To analyze the parameters γ and α, the images LI66 and LI67 were enhanced by the LIEST algorithm using different γ and α values.

The different enhanced images of LI66 using different γ values are presented in Fig. 12, and the difference value curves for the evaluation indicators of the original and enhanced LI66 images with different γ values are presented in Fig. 13.

In Fig. 12, the upper row presents the illumination maps corresponding to different γ values, and the lower row presents the original image and the corresponding enhanced images. As the value of γ increased, the illumination maps became darker, and the enhanced images became brighter. In other words, the greater the value of γ, the higher the contrast of the enhanced image.

In Fig. 13, the ''evaluation indicator'' denotes the difference value between the enhanced image and the original image; in Fig. 13(at), the values of the curves are smaller, and the effects of the enhanced image are better. However, in Fig. 13(b), the values of the curves are larger, and the effects of the enhanced image are better.

As presented in Fig. 13(a), with the increase of γ, the Sigma^2 values of the enhanced images hardly changed, but the NIQE values of the enhanced images fluctuated.

As presented in Fig. 13(b), with the increase of γ, the MLE values of the enhanced images hardly changed, but the MLSD and BG values of the enhanced images first increased and then decreased, and the inflection points were at about $\gamma = 0.8$.

TABLE 4. Evaluation indicator data for different α values.

α	Sigma^2 (↓)	NIQE (↓)	MLSD (↑)	MLE (↑)	BG (↑)
0.05	0.45	2.64	12.06	3.57	40.55
0.15	0.40	2.60	11.49	3.43	38.63
0.25	0.38	2.66	11.19	3.34	37.90
0.35	0.37	2.78	10.96	3.26	37.39
0.45	0.36	2.91	10.75	3.21	36.97
0.55	0.35	3.00	10.56	3.13	36.65
0.75	0.33	3.21	10.21	2.96	36.09
0.95	0.32	3.26	9.91	2.84	35.60

Taking Figs. 12 and 13 into consideration, the value range of γ is recommended to be [0.5,0.8].

The evaluation indicators of image LI67 enhanced by the LIEST algorithm using different values of α are listed in Table 4.

According to Table 4, the Sigma^2 and BG values of the enhanced images changed only slightly for different values of α. With the increase of α, the Sigma^2 values of the enhanced images improved slightly, but the other evaluation indicators of the enhanced images worsened. Thus, the value range of α is recommended to be [0.1,0.15].

B. PARAMETERS RELATED TO NOISE SUPPRESSION

This section discusses the parameters related to noise suppression, including k_j in Eq. (13) and β in Eq. (14).

The shrinking thresholds of the bandpass direction subband coefficients are determined by k_j and β.

When an estimated value of noise in a low-light image is low, β can prevent the shrinkage threshold from being too low; its recommended value range is [0.001,0.01], and its value range corresponds to the variance range [0.25,2.5]. The larger the value of β, the stronger the noise suppression effect of the LIEST algorithm. However, if the value of β is too large, some small details of the enhanced image will be lost. Experiments show that $\beta = 0.0035$ basically takes into account both noise suppression and weak detail retention. In this paper, its value was taken as 0.0035, and the variance corresponds to 0.89. In other words, when the noise variance of a low-light image is less than 0.89, $0.0035k_j\hat{\sigma}_{j,s}$ is used as the shrinkage threshold.

According to wavelet theory and geometric multiresolution analysis theory, the noise of an image is mainly concentrated in the high-frequency subband coefficients. Therefore, LIEST achieves noise suppression by shrinking the bandpass direction subband coefficient, that is, suppressing noise at the second to fourth decomposition scales.

In the following investigation, the values of the threshold coefficients of the second and third decomposition scales (k_2 and k_3) were set as equal. The values of k_2, k_3, and k_4 from 2 to 4 are subsequently discussed according to the 3 times variance as the center.

The Sigma^2 and NIQE curves of the enhanced LI68 images with different threshold coefficients are presented in Fig. 14.

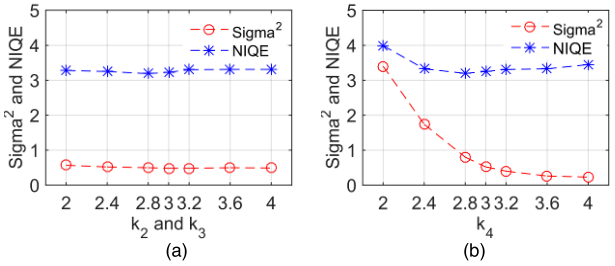

FIGURE 14. The Sigma^2 and NIQE curves of the enhanced LI68 images with different threshold coefficients. (a) The Sigma^2 and NIQE curves with different k_2 and k_3 values at $k_4 = 3$; (b) The Sigma^2 and NIQE curves with different k_4 values at $k_2 = 2.4$ and $k_3 = 2.4$.

FIGURE 15. Comparison of enhanced images and the original image corresponding to different values of k_4.

The original Sigma^2 and NIQE values of image LI68 were 5.04 and 4.98, respectively.

It can be seen from Figs. 14(a) and 14(b) that the value of k_4 (within the recommended value range) has a greater effect on the Sigma^2 and NIQE values of the enhanced image, while the values of k_2 and k_3 have lesser effects on the Sigma^2 and NIQE values of the enhanced image.

In Fig. 14(b), the Sigma^2 curve monotonously decreases. However, the curve of NIQE first drops and then rises, which indicates that the quality of the enhanced image was first improved and then decreased. Thus, after comprehensive consideration of the Sigma^2 and NIQE evaluation indicators, k_2, k_3, and k_4 are respectively set as 2.4, 2.4, and 3.

Fig. 15 presents the enhanced LI68 images when k_2 and k_3 were 2.4, and k_4 was set as 2, 3, and 4, respectively.

The enhancement effects of all enhanced images presented in Fig. 15 are very significant, but the local details of the enhanced images have some differences; the image enhanced using $k_4 = 2$ has more residual noise, but that using $k_4 = 4$ has more detail loss. The enhanced image using $k_4 = 3$ takes into account both noise suppression and detail retention.

C. DISCUSSION

The algorithm presented in this paper can not only improve the contrast of low-light images, but also achieves noise suppression and specific detail-highlighting. Compared with other algorithms used for enhancing low-light images, the proposed LIEST algorithm is more suitable for enhancing low-light images with noise. However, there remain some imperfections in LIEST; for example, its enhancement speed must be further improved, and its parameters require further optimization.

VI. CONCLUSION

According to the conducted experiments, the following conclusions can be drawn.

Illumination map estimation can be well implemented in the shearlet transform domain. Additionally, the noise of the final enhanced image can be suppressed by shrinking the bandpass direction subband coefficients of the original image in the NSST domain, which avoids the risk of the amplified noise overwhelming the details in the image enhancement process. Finally, not only can the LIEST algorithm improve the contrast of low-light images, but it can also achieve noise suppression and specific direction highlighting, and it exhibits good adaptability and stability.

REFERENCES

[1] Y.-F. Wang, H.-M. Liu, and Z.-W. Fu, "Low-light image enhancement via the absorption light scattering model," *IEEE Trans. Image Process.*, vol. 28, no. 11, pp. 5679–5690, Nov. 2019, doi: 10.1109/TIP.2019.2922106.

[2] F. Luo, L. Zhang, X. Zhou, T. Guo, Y. Cheng, and T. Yin, "Sparse-adaptive hypergraph discriminant analysis for hyperspectral image classification," *IEEE Geosci. Remote Sens. Lett.*, early access, Sep. 10, 2019, doi: 10.1109/LGRS.2019.2936652.

[3] F. Luo, B. Du, L. Zhang, L. Zhang, and D. Tao, "Feature learning using spatial-spectral hypergraph discriminant analysis for hyperspectral image," *IEEE Trans. Cybern.*, vol. 49, no. 7, pp. 2406–2419, Jul. 2019, doi: 10.1109/TCYB.2018.2810806.

[4] X. Wang and L. Chen, "Contrast enhancement using feature-preserving bi-histogram equalization," *Signal, Image Video Process.*, vol. 12, no. 4, pp. 685–692, May 2018, doi: 10.1007/s11760-017-1208-2.

[5] W. Wu, X. Yang, H. Li, K. Liu, L. Jian, and Z. Zhou, "A novel scheme for infrared image enhancement by using weighted least squares filter and fuzzy plateau histogram equalization," *Multimedia Tools Appl.*, vol. 76, no. 23, pp. 24789–24817, Dec. 2017, doi: 10.1007/s11042-017-4643-8.

[6] B. Xiao, H. Tang, Y. Jiang, W. Li, and G. Wang, "Brightness and contrast controllable image enhancement based on histogram specification," *Neurocomputing*, vol. 275, pp. 2798–2809, Jan. 2018, doi: 10.1016/j.neucom.2017.11.057.

[7] T. Arici, S. Dikbas, and Y. Altunbasak, "A histogram modification framework and its application for image contrast enhancement," *IEEE Trans. Image Process.*, vol. 18, no. 9, pp. 1921–1935, Sep. 2009.

[8] G. Jiang, S. C. F. Lin, C. Y. Wong, M. A. Rahman, T. R. Ren, N. Kwok, H. Shi, Y.-H. Yu, and T. Wu, "Color image enhancement with brightness preservation using a histogram specification approach," *Optik*, vol. 126, no. 24, pp. 5656–5664, Dec. 2015, doi: 10.1016/j.ijleo.2015.08.173.

[9] Y. Liu, H. Yan, S. Gao, and K. Yang, "Criteria to evaluate the fidelity of image enhancement by MSRCR," *IET Image Process.*, vol. 12, no. 6, pp. 880–887, Jun. 2018, doi: 10.1049/iet-ipr.2017.0171.

[10] S. Zhang, T. Wang, J. Dong, and H. Yu, "Underwater image enhancement via extended multi-scale Retinex," *Neurocomputing*, vol. 245, pp. 1–9, Jul. 2017, doi: 10.1016/j.neucom.2017.03.029.

[11] F. Tao, X. Yang, W. Wu, K. Liu, Z. Zhou, and Y. Liu, "Retinex-based image enhancement framework by using region covariance filter," *Soft Comput.*, vol. 22, no. 5, pp. 1399–1420, Mar. 2018, doi: 10.1007/s00500-017-2813-2.

[12] E. H. Land and J. J. McCann, "Lightness and Retinex theory," *J. Opt. Soc. Amer.*, vol. 61, no. 1, pp. 1–11, Jan. 1971, doi: 10.1364/JOSA.61.000001.

[13] X. Ye, G. Wu, L. Huang, F. Fan, and Y. Zhang, "Image enhancement for inspection of cable images based on Retinex theory and fuzzy enhancement method in wavelet domain," *Symmetry*, vol. 10, no. 11, p. 570, Nov. 2018, doi: 10.3390/sym10110570.

[14] C. Wu, Z. Liu, and H. Jiang, "Choosing the filter for catenary image enhancement method based on the non-subsampled contourlet transform," *Rev. Sci. Instrum.*, vol. 88, no. 5, May 2017, Art. no. 054701, doi: 10.1063/1.4983375.

[15] W. Wang and C. He, "A variational model with barrier functionals for Retinex," *SIAM J. Imag. Sci.*, vol. 8, no. 3, pp. 1955–1980, Jan. 2015, doi: 10.1137/15M1006908.

[16] L. LiuZ Pang and Y. Duan, "Retinex based on exponent-type total variation scheme," *Inverse Problems Imag.*, vol. 12, no. 5, pp. 1199–1217, 2018, doi: 10.3934/ipi.2018050.

[17] J. M. Morel, A. B. Petro, and C. Sbert, "A PDE formalization of Retinex theory," *IEEE Trans. Image Process.*, vol. 19, no. 11, pp. 2825–2837, Nov. 2010, doi: 10.1109/TIP.2010.2049239.
[18] Y.-F. Pu, P. Siarry, A. Chatterjee, Z.-N. Wang, Z. Yi, Y.-G. Liu, J.-L. Zhou, and Y. Wang, "A fractional-order variational framework for Retinex: Fractional-order partial differential equation-based formulation for multi-scale nonlocal contrast enhancement with texture preserving," *IEEE Trans. Image Process.*, vol. 27, no. 3, pp. 1214–1229, Mar. 2018, doi: 10.1109/TIP.2017.2779601.
[19] X. Fu, D. Zeng, Y. Huang, X.-P. Zhang, and X. Ding, "A weighted variational model for simultaneous reflectance and illumination estimation," in *Proc. IEEE Conf. Comput. Vis. Pattern Recognit. (CVPR)*, Jun. 2016, pp. 2782–2790, doi: 10.1109/CVPR.2016.304.
[20] Z. Feng and S. Hao, "Low-light image enhancement by refining illumination map with self-guided filtering," in *Proc. IEEE Int. Conf. Big Knowl. (ICBK)*, Aug. 2017, pp. 183–187, doi: 10.1109/ICBK.2017.37.
[21] S. A. Priyanka, Y.-K. Wang, and S.-Y. Huang, "Low-light image enhancement by principal component analysis," *IEEE Access*, vol. 7, pp. 3082–3092, 2019.
[22] Z. Rahman, M. Aamir, Y.-F. Pu, F. Ullah, and Q. Dai, "A smart system for low-light image enhancement with color constancy and detail manipulation in complex light environments," *Symmetry*, vol. 10, no. 12, p. 718, Dec. 2018, doi: 10.3390/sym10120718.
[23] S.-Y. Yu and H. Zhu, "Low-illumination image enhancement algorithm based on a physical lighting model," *IEEE Trans. Circuits Syst. Video Technol.*, vol. 29, no. 1, pp. 28–37, Jan. 2019.
[24] S. Ko, S. Yu, S. Park, B. Moon, W. Kang, and J. Paik, "Variational framework for low-light image enhancement using optimal transmission map and combined ℓ_1 and ℓ_2-minimization," *Signal Process., Image Commun.*, vol. 58, pp. 99–110, Oct. 2017.
[25] S. Hao, Y. Guo, and Z. Wei, "Lightness-aware contrast enhancement for images with different illumination conditions," *Multimedia Tools Appl.*, vol. 78, no. 3, pp. 3817–3830, Feb. 2019.
[26] S. Hao, Z. Feng, and Y. Guo, "Low-light image enhancement with a refined illumination map," *Multimedia Tools Appl.*, vol. 77, no. 22, pp. 29639–29650, Nov. 2018.
[27] S. Ma, H. Ma, Y. Xu, S. Li, C. Lv, and M. Zhu, "A low-light sensor image enhancement algorithm based on HSI color model," *Sensors*, vol. 18, no. 10, p. 3583, 2018.
[28] C. Tang, Y. Wang, H. Feng, Z. Xu, Q. Li, and Y. Chen, "Low-light image enhancement with strong light weakening and bright halo suppressing," *IET Image Process.*, vol. 13, no. 3, pp. 537–542, Feb. 2019.
[29] X. Guo, Y. Li, and H. Ling, "LIME: low-light image enhancement via illumination map estimation," *IEEE Trans. Image Process.*, vol. 26, no. 2, pp. 982–993, Feb. 2017, doi: 10.1109/TIP.2016.2639450.
[30] Z. Farbman, R. Fattal, D. Lischinski, and R. Szeliski, "Edge-preserving decompositions for multi-scale tone and detail manipulation," *ACM Trans. Graph.*, vol. 27, no. 3, pp. 1–10, Aug. 2008, doi: 10.1145/1360612.1360666.
[31] Y. Cho, J. Jeong, and A. Kim, "Model assisted multi-band fusion for single image enhancement and applications to robot vision," *IEEE Robot. Autom. Lett.*, vol. 3, no. 4, pp. 2822–2829, Jun. 2018, doi: 10.1109/LRA.2018.2843127.
[32] M. Li, J. Liu, W. Yang, X. Sun, and Z. Guo, "Structure-revealing low-light image enhancement via robust Retinex model," *IEEE Trans. Image Process.*, vol. 27, no. 6, pp. 2828–2841, Jun. 2018, doi: 10.1109/TIP.2018.2810539.
[33] S. Yi, D. Labate, G. R. Easley, and H. Krim, "A shearlet approach to edge analysis and detection," *IEEE Trans. Image Process.*, vol. 18, no. 5, pp. 929–941, May 2009.
[34] K. Guo and D. Labate, "Detection of singularities by discrete multiscale directional representations," *J. Geometric Anal.*, vol. 28, no. 3, pp. 2102–2128, Jul. 2018, doi: 10.1007/s12220-017-9897-x.
[35] B. Funt, F. Ciurea, and J. McCann, "Retinex in MATLAB," *J. Electron. Imag.*, vol. 13, no. 1, pp. 48–57, Jan. 2004, doi: 10.1117/1.1636761.
[36] S. Wang, J. Zheng, H.-M. Hu, and B. Li, "Naturalness preserved enhancement algorithm for non-uniform illumination images," *IEEE Trans. Image Process.*, vol. 22, no. 9, pp. 3538–3548, Sep. 2013, doi: 10.1109/TIP.2013.2261309.
[37] Y. Ren, Z. Ying, T. H. Li, and G. Li, "LECARM: Low-light image enhancement using the camera response model," *IEEE Trans. Circuits Syst. Video Technol.*, vol. 29, no. 4, pp. 968–981, Apr. 2019, doi: 10.1109/TCSVT.2018.2828141.
[38] G. Fu, L. Duan, and C. Xiao, "A hybrid L_2-L_P variational model for single low-light image enhancement with bright channel prior," in *Proc. IEEE Int. Conf. Image Process. (ICIP)*, Taipei, Taiwan, Sep. 2019, pp. 1925–1929.
[39] A. B. Petro, C. Sbert, and J.-M. Morel, "Multiscale retinex," *Image Process. Line*, vol. 4, pp. 71–88, Apr. 2014, doi: 10.5201/ipol.2014.107.
[40] Y. P. Loh and C. S. Chan, "Getting to know low-light images with the exclusively dark dataset," *Comput. Vis. Image Understand.*, vol. 178, pp. 30–42, 2019, doi: 10.1016/j.cviu.2018.10.010.
[41] A. Mittal, R. Soundararajan, and A. C. Bovik, "Making a 'completely blind' image quality analyzer," *IEEE Signal Process. Lett.*, vol. 20, no. 3, pp. 209–212, Mar. 2013, doi: 10.1109/LSP.2012.2227726.
[42] A. Mittal, A. K. Moorthy, and A. C. Bovik, "No-reference image quality assessment in the spatial domain," *IEEE Trans. Image Process.*, vol. 21, no. 12, pp. 4695–4708, Dec. 2012, doi: 10.1109/TIP.2012.2214050.

MANLI WANG was born in Jiaozuo, China, in 1981. He received the B.S. degree in electrical engineering and automation and the M.S. degree in control theory and control engineering from Henan Polytechnic University. He is currently pursuing the Ph.D. degree with the School of Mechanical Electronic and Information Engineering, China University of Mining and Technology, Beijing, China. He has published a number of articles in image processing journals. His research interests include image denoising and image enhancement.

ZIJIAN TIAN was born in Hunan, China, in 1964. He received the B.S. degree from the Xi'an Mining Institute, Xi'an, China, in 1986, and the M.S. and Ph.D. degrees in communications and information systems from the China University of Mining and Technology, Beijing, China, in 1995 and 2004, respectively. He is currently a Professor with the China University of Mining and Technology. His research interests include multimedia systems and image processing. He has published two books and more than 20 articles in these related fields.

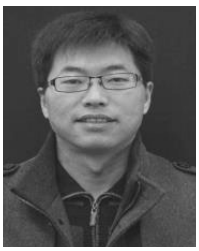

WEIFENG GUI was born in China, in 1976. He received the M.S. degree in educational technology from Henan Normal University. He is currently working with Henan Polytechnic University.

XIANGYANG ZHANG was born in China, in 1970. He is currently an Engineer with the China University of Mining and Technology, Beijing. His research interests include image processing and information security.

WENQING WANG was born in 1963. He is currently a Professor of engineering. His research interest includes mine intelligent instrument.